

Article

Electrochemical Detection of Tumor Cell-Derived Exosomes Based on Cyclic Enzyme Scission and Hybridization Chain Reaction Dual-Signal Amplification

Die Sun, Qunqun Guo, Hui Zhang * and Chenxin Cai

Jiangsu Key Laboratory of New Power Batteries, Jiangsu Collaborative Innovation Center of Biomedical Functional Materials, School of Chemistry and Materials Science, Nanjing Normal University, Nanjing 210023, China

* Correspondence: zhangh@nju.edu.cn

Abstract: Tumor cell-derived exosomes are considered a potential source of cancer biomarkers. Here, we developed an electrochemical sensing platform for the rapid and simple detection of exosomes, using the CCRF-CEM exosome as a model. The platform utilizes cyclic nicking enzyme cleavage and a hybridization chain reaction (HCR) for dual-signal amplification. A hairpin aptamer probe (HAP) containing an aptamer was designed for the assay. The specific binding between the aptamer and PTK7, present on the exosome surface, causes a conformational change in the HAP. This facilitates hybridization between the HAP and the linker DNA, which subsequently triggers cyclic cleavage of the nicking endonuclease towards the linker DNA. Therefore, exosome detection is transformed into DNA detection. By combining this approach with HCR signal amplification, we achieved high-sensitivity electrochemical detection of CCRF-CEM exosomes, down to 1.1×10^4 particles/mL. Importantly, this assay effectively detected tumor exosomes in complex biological fluids, demonstrating the potential for clinical diagnosis.

Keywords: exosomes; electrochemistry; cyclic enzyme scission; hybridization chain reaction



Citation: Sun, D.; Guo, Q.; Zhang, H.; Cai, C. Electrochemical Detection of Tumor Cell-Derived Exosomes Based on Cyclic Enzyme Scission and Hybridization Chain Reaction Dual-Signal Amplification.

Chemosensors **2023**, *11*, 415. <https://doi.org/10.3390/chemosensors11070415>

Academic Editor: Gyözö G. Láng

Received: 24 June 2023

Revised: 20 July 2023

Accepted: 21 July 2023

Published: 23 July 2023



Copyright: © 2023 by the authors. Licensee MDPI, Basel, Switzerland. This article is an open access article distributed under the terms and conditions of the Creative Commons Attribution (CC BY) license (<https://creativecommons.org/licenses/by/4.0/>).

1. Introduction

Exosomes are small extracellular vesicles, ranging in size from 30 to 150 nm. They are released by various cell types and are present in most body fluids including breast milk, tears, blood, etc. [1,2]. Similar to cells, exosomes have a phospholipid bilayer structure containing diverse proteins, nucleic acids (DNA and RNA), and lipids [3,4]. In body fluids, exosomes act as carriers, transporting functional information to neighboring or distant cells and facilitating cell-to-cell communication without direct contact. This communication mode is crucial for the exchange of materials between cells [5,6].

Tumor cell-derived exosomes represent a potential source of cancer biomarkers and can be utilized for tumor screening by detecting relevant exosomal information [7]. Additionally, the exosome surface contains various membrane proteins that can serve as markers for tumor generation and reproduction [8,9]. Consequently, developing an efficient and sensitive detection platform for analyzing tumor cell-derived exosomes and their surface proteins is highly valuable for applications in areas such as basic research, clinical diagnosis, and molecular therapy [10–12].

Currently, many methods have been developed for detecting exosomes, including nanoparticle tracking analysis (NTA) [13], surface-enhanced Raman spectroscopy (SERS) [14–16], fluorescence [17–19], and electrochemical methods [20–23]. Among these techniques, electrochemical methods have gained considerable interest due to their simplicity, portability, affordability, wide measurement range, and high sensitivity [20–24]. For instance, Wang et al. [20] immobilized DNA tetrahedrons containing aptamers on the working electrode surface to capture exosomes derived from hepatoma cells, using the

[Fe(CN)₆]^{3−/4−} redox couple for signal generation. Zhou et al. [21] immobilized thiolated anti-EpCAM aptamers on the working electrode to capture exosomes and used electrochemical signal probes consisting of Ag nanoparticles modified with anti-EpCAM aptamers and Cu nanoparticles modified with anti-PSMA aptamers for exosome detection. They also compared the expression levels of EpCAM and PSMA on the exosomes.

To enhance sensitivity, various signal amplification strategies have been used, including enzymatic amplification [25,26], DNA hybridization chain reaction (HCR) [27,28], DNA primer exchange reaction (PER) [29], hemin/G-quadruplex [30] and nanoparticles [23]. However, most of these methods involve the direct capture of exosomes by aptamers or antibodies on the electrode surface. The captured exosomes on the electrode surface can hinder electron transfer, which is unfavorable to electrochemical detection. To address this issue, several indirect detection methods have been developed. For example, our group [22] converted exosomes detection into DNA detection by employing aptamer recognition of exosomes. In this approach, the aptamer and partially complementary mDNA were modified on magnetic beads. The exosomes could specifically bind to the aptamer, resulting in the release of triple the amount of mDNA to amplify the signal. The signal was further amplified by adding exonuclease III for auxiliary circulation. This sensor offers a promising platform for highly sensitive detection of exosomes derived from human prostate tumor cells, with a detection limit of 7×10^4 particles/mL. Zhao et al. [31] have developed a signal amplified electrochemical method for exosome detection. The electrochemical signal was amplified by a three-dimensional DNA walker and exonuclease III-assisted signal amplification.

Herein, we report an electrochemical strategy for detecting tumor cell-derived exosomes using cyclic nicking enzyme cleavage and a hybridization chain reaction (HCR) for dual-signal amplification. We used CCRF-CEM exosomes as a model, together with tyrosine kinase-like 7 (PTK7), abundant on CCRF-CEM exosome membranes [32], as the target protein. A hairpin aptamer probe (HAP) was designed to contain the aptamer sequence sgc8 and a sequence complementary to the linker DNA, enabling conformational changes triggered by the target protein. In the presence of CCRF-CEM exosomes, sgc8 specifically bound PTK7 on the exosome membrane, causing HAP conformational changes that expose the hybridization region. The linker DNA hybridized to this HAP region, initiating nicking endonuclease-assisted cycling cleavage. Thus, small exosome quantities generated many cleaved DNA fragments (S1). Consequently, exosome detection became DNA detection. Combined with HCR amplification, the highly sensitive electrochemical detection of CCRF-CEM exosomes was achieved. Compared to previous work [22], this indirect detection strategy produces a signal DNA S1 based on HAP conformational changes, eliminating magnetic bead modification, separation and washing as well as making the method more convenient and concise. Additionally, this work has a lower detection limit (1.1×10^4 particles/mL) and wider linear range ($8.0 \times 10^4 \sim 3.2 \times 10^8$ particles/mL).

2. Experimental Section

2.1. Materials and Reagents

Nicking endonuclease Nb.BbvCI and $10 \times$ NEBuffer were obtained from New England Biolabs (Ipswich, MA, USA). Tris (2-carboxyethyl) phosphine hydrochloride (TCEP) was purchased from Aladdin (Shanghai, China). 6-Mercapto-1-hexanol (MCH) was obtained from Sigma-Aldrich (St. Louis, MO, USA). The plasma samples from healthy mice were obtained from Jiangsu KeyGen Biotech. Co., Ltd. (Nanjing, China). RPMI-1640 medium, DMEM medium and the HPLC-purified synthetic oligonucleotides were obtained from the Sangon Biotechnology Co., Ltd. (Shanghai, China). The sequences of these oligonucleotides are listed in Table 1. All other chemicals used were of analytical grade.

A 0.1 M phosphate buffer solution (PBS) at pH 7.4, supplemented with 0.1 M NaCl, was used as the immobilization buffer. A 10 mM PBS solution at pH 7.4 containing 0.1 M NaCl was used for cleaning the gold electrode. A 10 mM Tris-HCl buffer at pH 7.4, supplemented with 5 μ M hexaammineruthenium(III) chloride (RuHex), was used for electrochemical

detection. All aqueous solutions were prepared using 18 M Ω -cm deionized water from a Millipore water purification system.

Table 1. The sequences of the DNA used in this work *.

Name	Sequence (5'-3')
HAP	ATC TAA CTG CTG CGC CGC CGG GAA AAT ACT GTA CGG TTA <i>GAA AAA AAA AAA AAT CCT CAG CAG TTA</i>
Linker DNA	TCA GCA GGG AGG AAG ACA ATA TTA ACT <i>GCΔT</i> GAG GAT AAA CG
Capture DNA	CGC AGT TAA TAT TGT C
Hairpin H1	TTC CTC CCT GCT GAC ACA GAT CAG CAG GG
Hairpin H2	TCA GCA GGG AGG AAC CCT GCT GAT CTG TG

* The sequence in bold is the sequence of aptamer sgc8. The sequence in *italic* is the recognition sequence of nicking endonuclease Nb.BbvCI. " Δ " is the nicking site.

2.2. Apparatus

Exosome collection was performed by ultracentrifugation using an Optima XPN (Beckman Coulter, Indianapolis, IN, USA). Transmission electron microscopy (TEM) was performed using a JEOL-2010 microscope operating at 120 kV. Exosome was negative stained with 3% uranyl acetate solution. Nanoparticle tracking analysis (NTA) was done with a ZetaView from Particle Metrix, Germany. Polyacrylamide gel electrophoresis (PAGE) used a JY600C electrophoresis apparatus and gel imaging with a Tanon-3500 system (Shanghai, China). Differential pulse voltammetry (DPV) was carried out on a CHI 760C electrochemical system (Chenhua, Shanghai, China) using a three-electrode setup with a Pt wire counter electrode, saturated calomel reference electrode (SCE), and modified gold working electrode.

2.3. Cell Culture and Exosome Extraction

All cells were incubated under standard cell culture conditions (5% CO₂ at 37 °C). CCRF-CEM (T-lymphoblast, human acute lymphoblastic leukemia) and Ramos (B-lymphocyte, human Burkitt's lymphoma) cells were cultured in an RPMI-1640 medium, while HeLa (human cervix carcinoma) cells were cultured in a DMEM medium. Both culture media were supplemented with 10% fetal bovine serum (FBS) and 100 IU/mL penicillin-streptomycin. Exosomes from different tumor cells were extracted by ultracentrifugation [33,34] as follows: After 48 h of culture in a serum-free medium, tumor cells were collected and centrifuged at 300 \times g for 10 min to remove dead cells. The resulting supernatant was centrifuged at 16,500 \times g for 20 min and filtered through a 0.22 μ m filter. To precipitate the exosomes, the supernatant was ultracentrifuged at 110,000 \times g for 2 h and then washed with PBS. Finally, the collected exosomes were resuspended in PBS and stored at -80 °C until use. The plasma sample was subjected to ultracentrifugation at 110,000 \times g for 2 h, and the supernatant was collected as exosome-free plasma. All centrifugation steps were performed at 4 °C.

2.4. Detection Protocol

Before assembly, the 2 mm diameter gold electrode underwent pretreatment following a previously published method [35]. Briefly, the gold electrode was firstly polished to a mirror surface with 0.3 and 0.05 μ m alumina slurry on a polishing cloth, followed by ultrasonic cleaning in ethanol and deionized water, respectively. The gold electrode was then immersed in a freshly prepared piranha solution for 15 min. After being washed thoroughly with deionized water, the electrode was electrochemically cleaned in a 0.5 M H₂SO₄ with a potential scan from -0.2 V to 1.7 V until a remarkable cyclic voltammetry was obtained. Finally, the electrode was soaked in ethanol for 0.5 h and then rinsed with a copious amount of deionized water and dried with nitrogen.

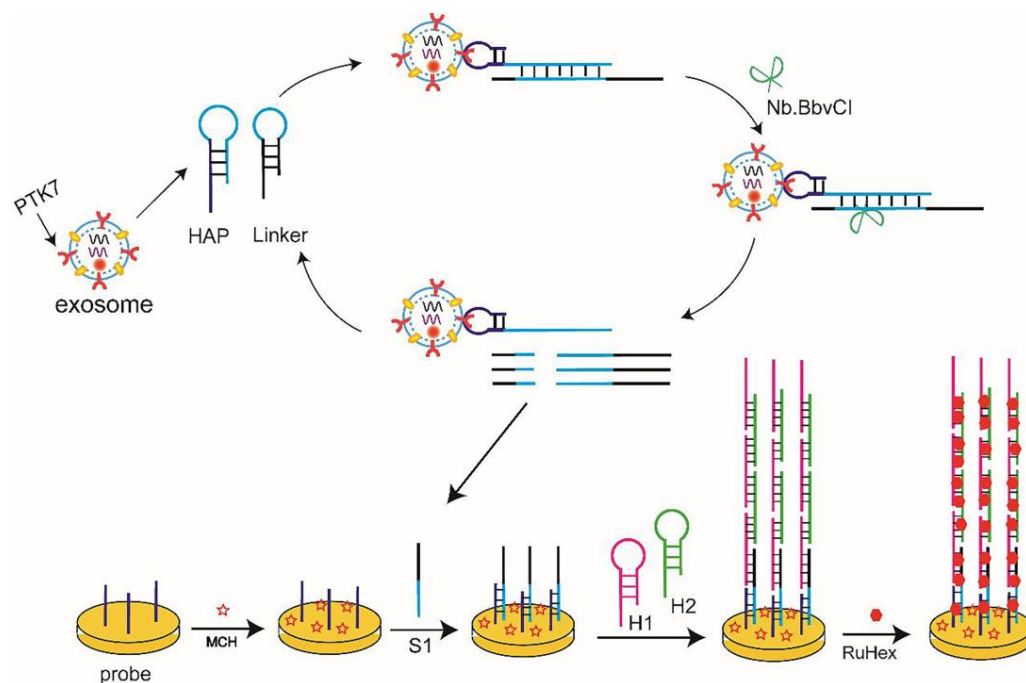
The HAP and linker DNA were heated to 95 °C for 5 min and cooled to room temperature to facilitate formation of a stable hairpin structure. Next, 10 µL of 0.5 µM thiolated probe DNA was dropped on the pre-treated gold electrode for assembly for 13 h at 4 °C. The electrode was then thoroughly rinsed with 10 mM PBS buffer. Subsequently, it was blocked with 1 mM MCH for 1 h at room temperature to eliminate nonspecific adsorption on the gold electrode surface. After thorough washing with 10 mM PBS, the gold electrode was stored at 4 °C for subsequent use.

The HAP (10 µM) and linker DNA (10 µM) were mixed with varying concentrations of exosomes at room temperature for 1 h to form aptamer–exosome complexes. Subsequently, 10 U of Nb.BbvCI and 10 × NEBuffer were added and incubated for 1 h. The gold electrode modified with probe DNA and MCH was then immersed in this solution and incubated at 37 °C for 1 h. The electrode was then thoroughly washed with 10 mM PBS and dried with nitrogen gas. Next, the electrode was immersed in 50 µL of freshly prepared reaction buffer containing H1 (0.5 µM) and H2 (0.5 µM) and incubated at room temperature for 2 h. After thorough washing with 10 mM PBS buffer, the electrode was immersed in Tris-HCl buffer containing RuHex for electrochemical measurements. Differential pulse voltammetry (DPV) measurements were performed by scanning the potential from −0.50 to +0.10 V, with a pulse amplitude of 50 mV and pulse width of 10 ms.

3. Results and Discussion

3.1. Mechanism of the Assay

In this study, the CCRF-CEM tumor cell-derived exosome was chosen as a model for the development of an electrochemical aptamer sensor. The detection mechanism is depicted in Scheme 1. The HAP used in this assay consists of two parts: the aptamer sgc8 (purple fragment) that specifically binds to the PTK7 protein (abundant on the CCRF-CEM exosome surface), and the hybridization region (light blue fragment) for signal amplification.



Scheme 1. Schematic of exosomes assay.

If no CCRF-CEM exosome is present, the sgc8 sequence of the HAP remains enclosed within the stem–loop structure, maintaining a stable configuration. Upon incubation with the CCRF-CEM exosomes, the sgc8 sequence of the HAP binds specifically to the PTK7 protein on the exosome membrane, leading to the conformational changes in the HAP and the release of the hybridization region. The released hybridization region opens

the stem-loop structure of the linker DNA and hybridizes with it, forming a double-stranded substrate for the nicking enzyme Nb.BbvCI. Nb.BbvCI cleaves the hybridized DNA fragment [36,37], resulting in the release of the cleaved DNA fragment (S1) and hybridization region into the solution. The free hybridization region can then hybridize with more linker DNA to initiate the cyclic cleavage of Nb.BbvCI toward the linker DNA, releasing numerous S1 sequences into the solution.

The cleaved DNA fragment S1 acts as the initiator for the HCR. It hybridizes with the probe DNA on the working electrode, and in the presence of the auxiliary hairpin DNA H1 and H2, the HCR process occurs, resulting in the formation of a long DNA double helix. RuHex, an electroactive substance, can be adsorbed onto the negatively charged DNA double helix structure through electrostatic interactions, generating high electrochemical signals [22,24]. The introduction of Nb.BbvCI-assisted cyclic scission and HCR dual signal amplification significantly enhances the detection sensitivity of the assay.

3.2. Characterization of the Exosomes

TEM analysis was conducted to characterize the size and morphology of the isolated CCRF-CEM exosomes. As depicted in Figure 1A, the TEM image reveals that the exosomes exhibit a characteristic cup-shaped morphology with an evident lipid bilayer membrane. The diameter of the exosomes ranges from 30 to 150 nm, which is consistent with reference values reported in the literature [31,34]. This confirms the successful collection of exosomes.

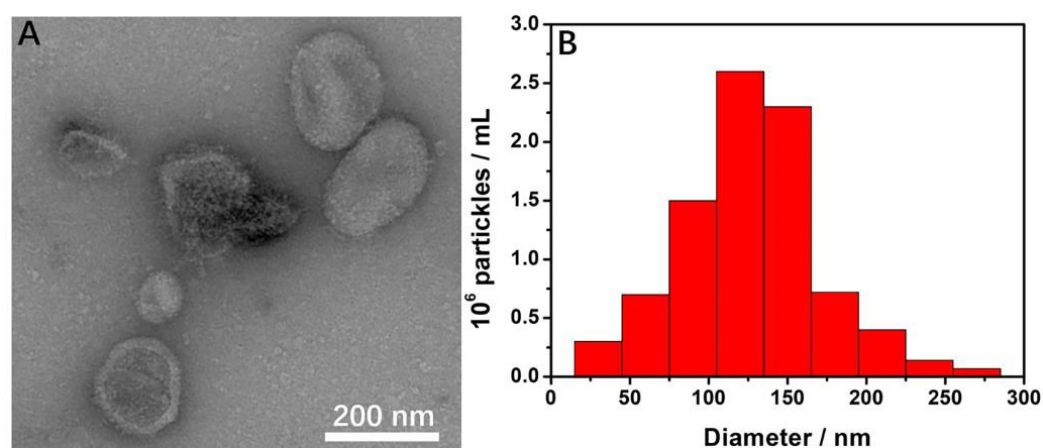


Figure 1. (A) TEM image and (B) particle size distribution of the extracted CCRF-CEM exosomes.

Additionally, NTA was employed to obtain the particle size distribution of the exosomes, as shown in Figure 1B. The *y*-axis represents the concentration of diluted exosomes, while the original concentration of exosomes was determined to be 1.6×10^9 particles/mL. The NTA results further support the successful isolation of exosomes.

3.3. Feasibility of the Assay

To evaluate the feasibility and effectiveness of the developed assay, the PAGE experiment was conducted. The results are presented in Figure 2.

In Figure 2A, it can be observed that in the absence of CCRF-CEM exosomes (lane 3), the HAP and linker DNA coexist without being cut by Nb.BbvCI, indicating that no hybridization occurs between the HAP and linker DNA without the presence of the target exosome. However, when CCRF-CEM exosomes were added and treated with Nb.BbvCI, the band corresponding to the linker DNA almost disappeared, and a new band appeared (lane 4). This observation suggests the target exosomes successfully trigger conformational changes in the HAP, leading to the formation of the exosome-aptamer complex and release of the hybridization region. Consequently, the stem of the linker DNA is opened by the hybridization region, allowing it to hybridize with the exosome-aptamer complex.

Nb.BbvCI then cleaves the hybridized DNA fragment, resulting in the release of S1 (new band in lane 4).

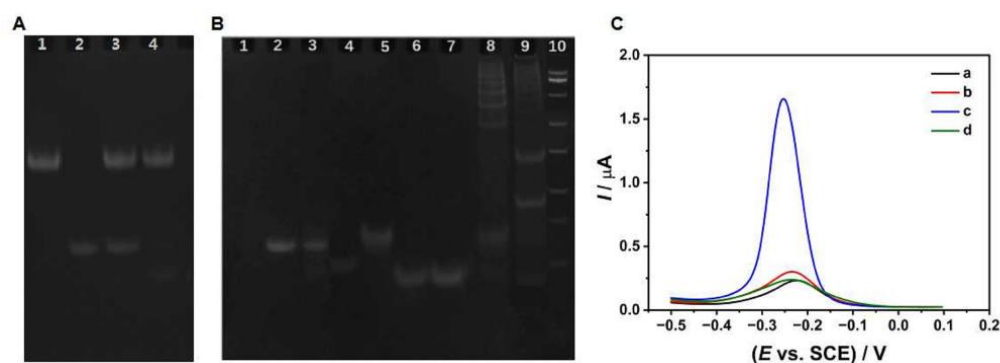


Figure 2. Gel electrophoresis of different samples: (A) lane 1, HAP; lane 2, linker DNA; lane 3, HAP + linker DNA + Nb.BbvCI; lane 4, HAP + linker DNA + Nb.BbvCI + CCRF-CEM exosomes; (B) Lane 1, probe DNA; lane 2, linker DNA; lane 3, probe DNA + linker DNA; Lane 4, S1; Lane 5, S1 + probe DNA; Lane 6, H1; Lane 7, H2; Lane 8, S1 + probe DNA + H1 + H2; Lane 9, HAP + linker DNA + Nb.BbvCI + CCRF-CEM exosomes + H1 + H2; Lane 10, DNA marker. (C) DPV response of gold electrode in different processes: (a) probe DNA/MCH-modified gold electrode; (b) incubation with CCRF-CEM exosomes, HAP, linker DNA and Nb.BbvCI; (c) further incubation with H1 and H2; (d) the probe DNA/MCH-modified gold electrode was treated with HAP, linker DNA and Nb.BbvCI, and then treated with H1 and H2.

Figure 2B provides further evidence of the assay's viability. Lane 3 is a mixture of the probe DNA and linker DNA. It clearly shows that the probe DNA does not hybridize with the linker DNA. However, in the presence of S1, hybridization occurs between the probe DNA and S1 (lane 5). Subsequently, S1 can further hybridize with H1 and H2, resulting in the generation of multiple new bands (lanes 8 and 9). This outcome confirms that the presence of the target exosomes successfully triggers the HCR.

Overall, the results from the PAGE experiment provide strong evidence supporting the feasibility of the proposed strategy for the detection of tumor cell-derived exosomes.

To further validate the feasibility of the developed strategy, DPV curves were recorded. As shown in Figure 2C, the gold electrode modified with the probe DNA and MCH exhibited a small cathodic peak (curve a). The small cathodic peak can be attributed to the electrochemical reduction of adsorbed RuHex to the probe DNA through electrostatic interactions [22,24]. After incubating the working electrode in the solution containing the target exosomes, HAP, linker DNA, and Nb.BbvCI, a slight increase in the peak current was observed (curve b). This increase is due to the successful triggering of HAP conformational changes by the target exosomes. The HAP then hybridizes with the linker DNA to generate the nicking site for Nb.BbvCI. Consequently, Nb.BbvCI cleaves the linker DNA, releasing S1 [36,37]. The released S1 further hybridizes with the probe DNA on the working electrode, and more RuHex molecules are absorbed, leading to an increase in the peak current.

Upon introduction of H1 and H2, a large cathodic peak is observed in curve c. This increase in the peak current can be attributed to the successful occurrence of the HCR triggered by the presence of S1. The HCR could result in the formation of a long DNA double-helix structure, facilitating the adsorption of many RuHex molecules onto the DNA through electrostatic interactions. This leads to a significantly amplified electrochemical signal. In curve d, when the target exosome is absent, the peak current remains relatively constant. This observation indicates that the HCR does not occur in the absence of target exosomes.

The DPV curves demonstrate the feasibility of the prepared electrochemical aptamer sensor for the detection of specific exosomes. The sensor utilizes the aptamer's specificity for the membrane protein of the exosomes, enabling the specific recognition and detection of the target exosomes.

Overall, the results from the PAGE and DPV experiments provide strong evidence supporting the feasibility of the proposed strategy for detecting tumor cell-derived exosomes.

3.4. Optimization of Experimental Conditions

In order to achieve excellent performance, the concentration and incubation time of Nb.BbvCI, as well as the concentrations of the probe DNA, H1, and H2, together with the HCR reaction time, were evaluated. Figure 3A illustrates the variation in the current with different concentrations of Nb.BbvCI. It can be observed that the current gradually increases with the increase in Nb.BbvCI concentration, reaching a relatively stable plateau at 10 U. Therefore, the optimal Nb.BbvCI concentration for the assay was determined to be 10 U.

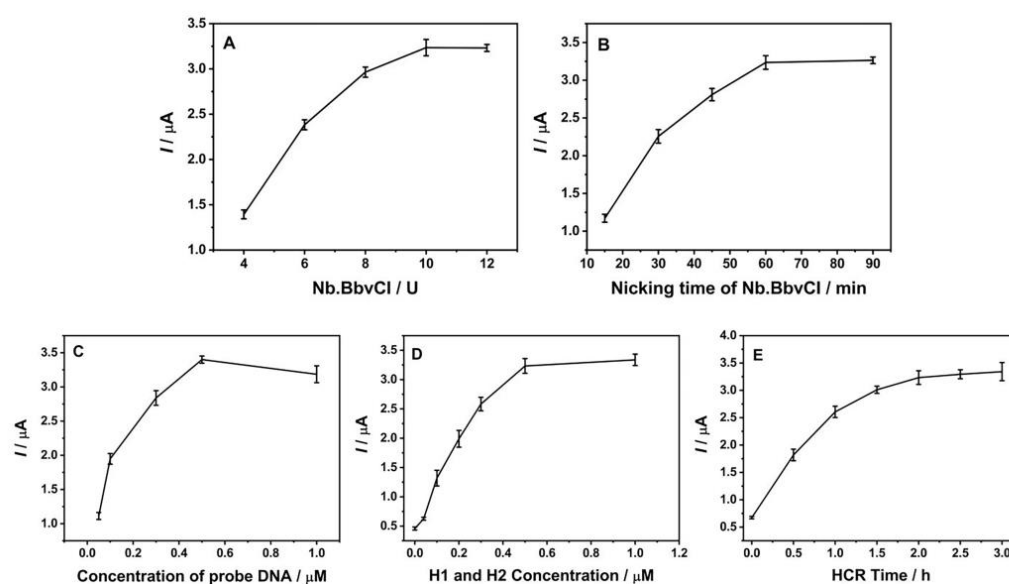


Figure 3. DPV signal was plotted as a function of (A) concentration of Nb.BbvCI, (B) nicking time of Nb.BbvCI and (C) concentration of probe DNA; (D) effects of H1 and H2 concentrations on HCR amplification and (E) effect of hybridization time on HCR amplification.

Subsequently, the effect of the nicking incubation time of Nb.BbvCI on the current was examined (Figure 3B). The current shows a significant increase with increasing incubation time, reaching a relatively stable plateau at 60 min. Therefore, the optimal nicking incubation time for Nb.BbvCI is determined to be 60 min.

In order to optimize the efficiency of the HCR, it is crucial to control the density of the probe DNA on the gold electrode surface. This density affects steric hindrance and, consequently, the efficiency of the hybridization process [38]. To determine the optimal probe DNA concentration, different concentrations were tested (Figure 3C). It can be observed that the peak current gradually increases with the increase in the probe DNA concentration, until reaching a maximum at 0.5 μM . However, when the concentration exceeds 0.5 μM , the peak current starts to decrease gradually. This decrease at higher probe DNA concentrations can be attributed to the limited surface area available for hybridization on the modified electrode, leading to a reduced HCR efficiency. Based on these results, the optimal probe DNA concentration is determined to be 0.5 μM .

Furthermore, the concentrations of H1 and H2, as well as the hybridization time, play a crucial role in the electrochemical signal generated by RuHex. Figure 3D demonstrates that increasing the H1 and H2 concentrations led to a significant increase in the current signal, reaching a maximum at 0.5 μM . Further concentration increases did not significantly affect the current. Figure 3E shows that the current signal gradually increases with longer hybridization time and eventually reaches a steady plateau after 2 h. Consequently, the optimal conditions for the HCR reaction were determined to be 0.5 μM for both H1 and H2 concentrations and a 2-h hybridization time.

3.5. CCRF-CEM Exosomes Detection

Under optimized conditions, various concentrations of CCRF-CEM exosomes were examined using the designed assay. As depicted in Figure 4A, the DPV signal displayed a gradual increase as the exosome concentration increased from 8.0×10^4 to 3.2×10^8 particles/mL. Figure 4B demonstrates that the DPV peak current changes (ΔI) exhibited a linear correlation with the logarithm of the exosome concentration, yielding a correlation coefficient (R^2) of 0.982. The linear regression equation was $\Delta I = -2.804 + 0.731 \lg c$, where ΔI represents the difference in the current signal between the initial and final states, and c represents the exosome concentration. The assay achieved a detection limit of approximately 1.1×10^4 particles/mL (3σ rule), indicating its sensitivity to CCRF-CEM exosome detection. Additionally, the assay outperformed some previous methods in terms of a broader linear range and lower detection limit, as summarized in Table 2. These findings highlight the enhanced sensitivity and improved dynamic range of the assay developed for exosome detection.

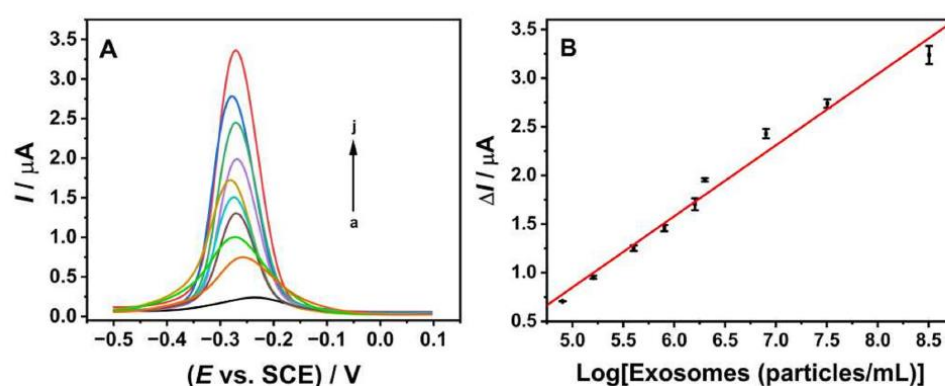


Figure 4. (A) DPV response of different concentrations of exosomes, the concentrations of exosomes from a to j are 0, 8.0×10^4 , 1.6×10^5 , 4.0×10^5 , 8.0×10^5 , 1.6×10^6 , 2.0×10^6 , 8.0×10^6 , 3.2×10^7 , 3.2×10^8 particles/mL; (B) Linear relationship between DPV signal changes and the logarithm of exosomes concentrations.

Table 2. Comparison of sensitivity and linear range of exosome detection methods.

Detection Method	Linear Range (Particles/mL)	LOD (Particles/mL)	Ref
electrochemical method	$1.0 \times 10^6 \sim 1.2 \times 10^8$	7.0×10^4	[22]
electrochemical method	$1 \times 10^6 \sim 1 \times 10^{11}$	1.58×10^5	[23]
electrochemical method	$2.47 \times 10^8 \sim 1.23 \times 10^9$	9.3×10^7	[39]
colorimetric method	$2.47 \times 10^8 \sim 2.47 \times 10^9$	7.1×10^8	[40]
fluorescence method	$8.3 \times 10^5 \sim 5.3 \times 10^7$	3.94×10^5	[17]
electrogenerated chemiluminescence	$1 \times 10^7 \sim 5 \times 10^8$	3.12×10^6	[41]
surface plasmon resonance	$1 \times 10^5 \sim 1 \times 10^8$	3×10^4	[42]
electrochemical method	$1.00 \times 10^5 \sim 1 \times 10^7$	1.00×10^5	[42]
electrochemical method	$8.0 \times 10^4 \sim 3.2 \times 10^8$	1.1×10^4	This work

3.6. Selective and Feasible Evaluation of the Proposed Strategy

To evaluate the selectivity of the developed assay, we conducted a specificity assessment using exosomes obtained from Ramos and HeLa tumor cells, as well as a PBS buffer solution as a control. Figure 5A illustrates that the PTK7 protein content in CCRF-CEM tumor cell-derived exosomes is much higher compared to exosomes from Ramos and HeLa tumor cells. Moreover, the DPV signal from the PBS solution, which lacks the PTK7 protein, was almost negligible, consistent with findings reported in the literature [32,43]. These results provide evidence of the assay's excellent selectivity, specifically targeting the

PTK7 protein in CCRF-CEM tumor cell-derived exosomes, and are potentially useful for clinical diagnosis.

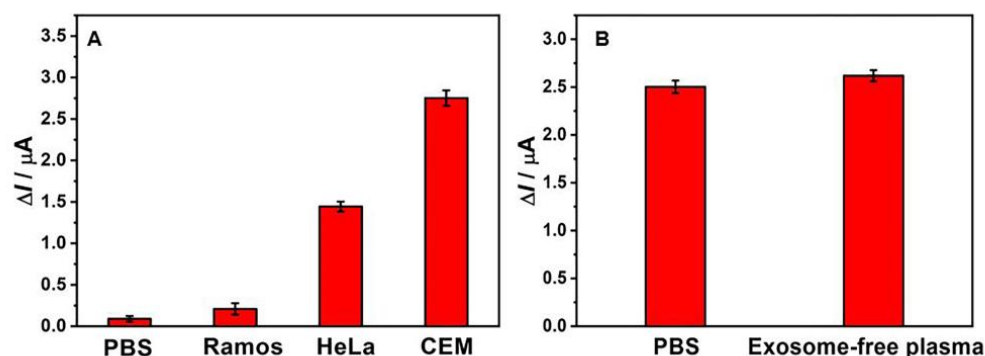


Figure 5. (A) DPV signal response of PTK7 content in different exosomes; (B) Analysis of the impact of complex environment on exosomes.

Furthermore, the reproducibility of the assay was evaluated by detecting CCRF-CEM exosomes at a concentration of 3.2×10^7 particles/mL using six parallel electrodes. The relative standard deviation (RSD) was about 2.41%. The results demonstrate the excellent reproducibility of the assay. This low RSD value highlights the consistency and reliability of the developed method for exosome detection.

To assess the feasibility of the sensing platform in real samples, we conducted detection and analysis using exosome-depleted plasma. In Figure 5B, we compare the DPV signals obtained by adding the same number of exosomes to the PBS buffer solution and exosome-depleted plasma under the same conditions. Remarkably, the current signal values detected in both environments exhibit negligible differences. This observation suggests the excellent feasibility and robust performance of the assay in complex biological matrices such as plasma, demonstrating its potential for exosome analysis in real samples.

To further validate the reliability of the assay in practical applications, we conducted tests by adding known concentrations of CCRF-CEM exosomes to exosome-depleted plasma. The detected final concentrations were 3.06×10^7 , 2.42×10^7 , 1.35×10^7 , and 5.90×10^6 particles/mL, respectively. The results presented in Table 3 demonstrate the robustness of the assay in complex environments. The calculated recovery rates ranged from 95.63% to 103.5%, indicating the accuracy of the method for quantifying exosome concentrations. Additionally, the RSD, with values below 3.48% ($n = 3$), underscores the excellent reproducibility of the assay in complex biological matrices. These findings further support the reliability and practical applicability of the assay in real-world scenarios.

Table 3. Exosomes were analyzed in exosome-removed plasma.

Number	Added (Particles/mL)	Count (Particles/mL)	Recovery (%)	RSD (%)
1	3.20×10^7	3.06×10^7	95.63	1.38
2	2.50×10^7	2.42×10^7	96.8	2.85
3	1.30×10^7	1.35×10^7	103.8	3.48
4	6.00×10^6	5.90×10^6	98.3	2.34

4. Conclusions

In this study, an electrochemical sensing platform for the detection of CCRF-CEM exosomes was successfully developed. The assay utilizes a dual signal amplification strategy by a combination of a cyclic nicking enzyme and a HCR, eliminating the need for exosome capture on the electrode surface. The method offers several advantages, including a wider linear range, high selectivity, and good reproducibility. Notably, the limit of detection was as low as 1.1×10^4 particles/mL. Importantly, the method demonstrated

applicability in complex plasma conditions, highlighting its potential for exosome-based research and diagnostic applications, especially in early clinical diagnosis of oncological diseases. This innovative approach holds promise for advancing exosome analysis and enhancing our understanding of tumor-related biomarkers.

Author Contributions: Experiment, data analysis, writing—original draft, D.S. and Q.G.; design and methodology, project instruction, funding acquisition, H.Z.; resources, writing—review and editing, H.Z. and C.C. All authors have read and agreed to the published version of the manuscript.

Funding: This research was funded by the National Natural Science Foundation of China (No. 22274077).

Institutional Review Board Statement: Not applicable.

Informed Consent Statement: Not applicable.

Data Availability Statement: The data are available upon request to the corresponding authors.

Conflicts of Interest: The authors declare no conflict of interest.

References

1. Raposo, G.; Stoorvogel, W. Extracellular vesicles: Exosomes, microvesicles, and friends. *J. Cell Biol.* **2013**, *200*, 373–383. [[CrossRef](#)] [[PubMed](#)]
2. Alptekin, A.; Parvin, M.; Chowdhury, H.I.; Rashid, M.H.; Arbab, A.S. Engineered exosomes for studies in tumor immunology. *Immunol. Rev.* **2022**, *312*, 76–102. [[CrossRef](#)] [[PubMed](#)]
3. Kalluri, R.; LeBleu, V.S. The biology, function, and biomedical applications of exosomes. *Science* **2020**, *367*, eaau6977. [[CrossRef](#)] [[PubMed](#)]
4. Pegtel, D.M.; Gould, S.J. Exosomes. *Annu. Rev. Biochem.* **2019**, *88*, 487–514. [[CrossRef](#)]
5. Stefanska, K.; Jozkowiak, M.; Angelova Volponi, A.; Shibli, J.A.; Golkar-Narenji, A.; Antosik, P.; Bukowska, D.; Piotrowska-Kempisty, H.; Mozdziak, P.; Dziegiel, P.; et al. The Role of Exosomes in Human Carcinogenesis and Cancer Therapy—Recent Findings from Molecular and Clinical Research. *Cells* **2023**, *12*, 356. [[CrossRef](#)]
6. Kalluri, R. The biology and function of exosomes in cancer. *J. Clin. Investig.* **2016**, *126*, 1208–1215. [[CrossRef](#)]
7. Guo, Y.; Ji, X.; Liu, J.; Fan, D.; Zhou, Q.; Chen, C.; Wang, W.; Wang, G.; Wang, H.; Yuan, W.; et al. Effects of exosomes on pre-metastatic niche formation in tumors. *Mol. Cancer* **2019**, *18*, 39. [[CrossRef](#)]
8. Zhang, J.; Zhu, Y.; Shi, J.; Zhang, K.; Zhang, Z.; Zhang, H. Sensitive Signal Amplifying a Diagnostic Biochip Based on a Biomimetic Periodic Nanostructure for Detecting Cancer Exosomes. *ACS Appl. Mater. Interfaces* **2020**, *12*, 33473–33482. [[CrossRef](#)]
9. Li, A.; Zhang, T.; Zheng, M.; Liu, Y.; Chen, Z. Exosomal proteins as potential markers of tumor diagnosis. *J. Hematol. Oncol.* **2017**, *10*, 175. [[CrossRef](#)]
10. Xu, B.; Chen, Y.; Peng, M.; Zheng, J.H.; Zuo, C. Exploring the potential of exosomes in diagnosis and drug delivery for pancreatic ductal adenocarcinoma. *Int. J. Cancer* **2023**, *152*, 110–122. [[CrossRef](#)]
11. Sun, Y.; Liu, J. Potential of cancer cell-derived exosomes in clinical application: A review of recent research advances. *Clin. Ther.* **2014**, *36*, 863–872. [[CrossRef](#)]
12. Hsu, M.T.; Wang, Y.K.; Tseng, Y.J. Exosomal Proteins and Lipids as Potential Biomarkers for Lung Cancer Diagnosis, Prognosis, and Treatment. *Cancers* **2022**, *14*, 732. [[CrossRef](#)] [[PubMed](#)]
13. Sharma, V.; Nikolajeff, F.; Kumar, S. Employing nanoparticle tracking analysis of salivary neuronal exosomes for early detection of neurodegenerative diseases. *Transl. Neurodegener.* **2023**, *12*, 7. [[CrossRef](#)] [[PubMed](#)]
14. Li, J.; Li, Y.; Li, P.; Zhang, Y.; Du, L.; Wang, Y.; Zhang, C.; Wang, C. Exosome detection via surface-enhanced Raman spectroscopy for cancer diagnosis. *Acta Biomater.* **2022**, *144*, 1–14. [[CrossRef](#)] [[PubMed](#)]
15. Park, J.; Hwang, M.; Choi, B.; Jeong, H.; Jung, J.-h.; Kim, H.K.; Hong, S.; Park, J.-h.; Choi, Y. Exosome Classification by Pattern Analysis of Surface-Enhanced Raman Spectroscopy Data for Lung Cancer Diagnosis. *Anal. Chem.* **2017**, *89*, 6695–6701. [[CrossRef](#)] [[PubMed](#)]
16. Shin, H.; Oh, S.; Hong, S.; Kang, M.; Kang, D.; Ji, Y.G.; Choi, B.H.; Kang, K.W.; Jeong, H.; Park, Y.; et al. Early-Stage Lung Cancer Diagnosis by Deep Learning-Based Spectroscopic Analysis of Circulating Exosomes. *ACS Nano* **2020**, *14*, 5435–5444. [[CrossRef](#)]
17. Xia, Y.; Chen, T.; Chen, G.; Weng, Y.; Zeng, L.; Liao, Y.; Chen, W.; Lan, J.; Zhang, J.; Chen, J. A nature-inspired colorimetric and fluorescent dual-modal biosensor for exosomes detection. *Talanta* **2020**, *214*, 120851. [[CrossRef](#)]
18. Zhou, J.; Lin, Q.; Huang, Z.; Xiong, H.; Yang, B.; Chen, H.; Kong, J. Aptamer-Initiated Catalytic Hairpin Assembly Fluorescence Assay for Universal, Sensitive Exosome Detection. *Anal. Chem.* **2022**, *94*, 5723–5728. [[CrossRef](#)]
19. Huang, R.; He, L.; Li, S.; Liu, H.; Jin, L.; Chen, Z.; Zhao, Y.; Li, Z.; Deng, Y.; He, N. A simple fluorescence aptasensor for gastric cancer exosome detection based on branched rolling circle amplification. *Nanoscale* **2020**, *12*, 2445–2451. [[CrossRef](#)]
20. Wang, S.; Zhang, L.; Wan, S.; Cansiz, S.; Cui, C.; Liu, Y.; Cai, R.; Hong, C.; Teng, I.T.; Shi, M.; et al. Aptasensor with Expanded Nucleotide Using DNA Nanotetrahedra for Electrochemical Detection of Cancerous Exosomes. *ACS Nano* **2017**, *11*, 3943–3949. [[CrossRef](#)] [[PubMed](#)]

21. Zhou, Y.G.; Mohamadi, R.M.; Poudineh, M.; Kermanshah, L.; Ahmed, S.; Safaei, T.S.; Stojcic, J.; Nam, R.K.; Sargent, E.H.; Kelley, S.O. Interrogating Circulating Microsomes and Exosomes Using Metal Nanoparticles. *Small* **2016**, *12*, 727–732. [[CrossRef](#)] [[PubMed](#)]
22. Dong, H.; Chen, H.; Jiang, J.; Zhang, H.; Cai, C.; Shen, Q. Highly Sensitive Electrochemical Detection of Tumor Exosomes Based on Aptamer Recognition-Induced Multi-DNA Release and Cyclic Enzymatic Amplification. *Anal. Chem.* **2018**, *90*, 4507–4513. [[CrossRef](#)] [[PubMed](#)]
23. Cheng, W.; Duan, C.; Chen, Y.; Li, D.; Hou, Z.; Yao, Y.; Jiao, J.; Xiang, Y. Highly Sensitive Aptasensor for Detecting Cancerous Exosomes Based on Clover-like Gold Nanoclusters. *Anal. Chem.* **2023**, *95*, 3606–3612. [[CrossRef](#)]
24. Bagheri Hashkavayi, A.; Cha, B.S.; Lee, E.S.; Kim, S.; Park, K.S. Advances in Exosome Analysis Methods with an Emphasis on Electrochemistry. *Anal. Chem.* **2020**, *92*, 12733–12740. [[CrossRef](#)]
25. Jeong, S.; Park, J.; Pathania, D.; Castro, C.M.; Weissleder, R.; Lee, H. Integrated Magneto-Electrochemical Sensor for Exosome Analysis. *ACS Nano* **2016**, *10*, 1802–1809. [[CrossRef](#)] [[PubMed](#)]
26. Ziaei, P.; Berkman, C.E.; Norton, M.G. Review: Isolation and Detection of Tumor-Derived Extracellular Vesicles. *ACS Appl. Nano Mater.* **2018**, *1*, 2004–2020. [[CrossRef](#)]
27. An, Y.; Jin, T.; Zhu, Y.; Zhang, F.; He, P. An ultrasensitive electrochemical aptasensor for the determination of tumor exosomes based on click chemistry. *Biosens. Bioelectron.* **2019**, *142*, 111503. [[CrossRef](#)]
28. Liu, X.; Gao, X.; Yang, L.; Zhao, Y.; Li, F. Metal-Organic Framework-Functionalized Paper-Based Electrochemical Biosensor for Ultrasensitive Exosome Assay. *Anal. Chem.* **2021**, *93*, 11792–11799. [[CrossRef](#)]
29. Huang, M.; Xiang, Y.; Chen, Y.; Lu, H.; Zhang, H.; Liu, F.; Qin, X.; Qin, X.; Li, X.; Yang, F. Bottom-Up Signal Boosting with Fractal Nanostructuring and Primer Exchange Reaction for Ultrasensitive Detection of Cancerous Exosomes. *ACS Sens.* **2023**, *8*, 1308–1317. [[CrossRef](#)]
30. Huang, R.; He, L.; Xia, Y.; Xu, H.; Liu, C.; Xie, H.; Wang, S.; Peng, L.; Liu, Y.; Liu, Y.; et al. A Sensitive Aptasensor Based on a Hemin/G-Quadruplex-Assisted Signal Amplification Strategy for Electrochemical Detection of Gastric Cancer Exosomes. *Small* **2019**, *15*, e1900735. [[CrossRef](#)]
31. Zhao, L.; Sun, R.; He, P.; Zhang, X. Ultrasensitive Detection of Exosomes by Target-Triggered Three-Dimensional DNA Walking Machine and Exonuclease III-Assisted Electrochemical Ratiometric Biosensing. *Anal. Chem.* **2019**, *91*, 14773–14779. [[CrossRef](#)] [[PubMed](#)]
32. Jiang, Y.; Shi, M.; Liu, Y.; Wan, S.; Cui, C.; Zhang, L.; Tan, W. Aptamer/AuNP Biosensor for Colorimetric Profiling of Exosomal Proteins. *Angew. Chem. Int. Ed.* **2017**, *56*, 11916–11920. [[CrossRef](#)] [[PubMed](#)]
33. Skog, J.; Wurdinger, T.; van Rijn, S.; Meijer, D.H.; Gainche, L.; Sena-Esteves, M.; Curry, W.T., Jr.; Carter, B.S.; Krichevsky, A.M.; Breakefield, X.O. Glioblastoma microvesicles transport RNA and proteins that promote tumour growth and provide diagnostic biomarkers. *Nat. Cell Biol.* **2008**, *10*, 1470–1476. [[CrossRef](#)] [[PubMed](#)]
34. Tosar, J.P.; Gambaro, F.; Sanguinetti, J.; Bonilla, B.; Witwer, K.W.; Cayota, A. Assessment of small RNA sorting into different extracellular fractions revealed by high-throughput sequencing of breast cell lines. *Nucleic Acids Res.* **2015**, *43*, 5601–5616. [[CrossRef](#)]
35. Zhang, J.; Song, S.; Wang, L.; Pan, D.; Fan, C. A gold nanoparticle-based chronocoulometric DNA sensor for amplified detection of DNA. *Nat. Protoc.* **2007**, *2*, 2888–2895. [[CrossRef](#)]
36. Zhang, X.; Xiao, K.; Cheng, L.; Chen, H.; Liu, B.; Zhang, S.; Kong, J. Visual and highly sensitive detection of cancer cells by a colorimetric aptasensor based on cell-triggered cyclic enzymatic signal amplification. *Anal. Chem.* **2014**, *86*, 5567–5572. [[CrossRef](#)]
37. Li, J.; Fu, H.E.; Wu, L.J.; Zheng, A.X.; Chen, G.N.; Yang, H.H. General colorimetric detection of proteins and small molecules based on cyclic enzymatic signal amplification and hairpin aptamer probe. *Anal. Chem.* **2012**, *84*, 5309–5315. [[CrossRef](#)]
38. Liu, Q.; Xie, X.L.; Mao, C.J.; Chen, J.S.; Niu, H.L.; Song, J.M. Electrochemiluminescent biosensor with DNA link for selective detection of human IgG based on steric hindrance. *Talanta* **2019**, *194*, 745–751. [[CrossRef](#)]
39. Kasetsirikul, S.; Tran, K.T.; Clack, K.; Soda, N.; Shiddiky, M.J.A.; Nguyen, N.T. Low-cost electrochemical paper-based device for exosome detection. *Analyst* **2022**, *147*, 3732–3740. [[CrossRef](#)]
40. Zhou, Y.; Xu, H.; Wang, H.; Ye, B.C. Detection of breast cancer-derived exosomes using the horseradish peroxidase-mimicking DNAzyme as an aptasensor. *Analyst* **2019**, *145*, 107–114. [[CrossRef](#)]
41. Zhang, H.; Wang, Z.; Wang, F.; Zhang, Y.; Wang, H.; Liu, Y. In Situ Formation of Gold Nanoparticles Decorated Ti₃C₂ MXenes Nanoprobe for Highly Sensitive Electrogenerated Chemiluminescence Detection of Exosomes and Their Surface Proteins. *Anal. Chem.* **2020**, *92*, 5546–5553. [[CrossRef](#)] [[PubMed](#)]
42. Chen, W.; Li, J.; Wei, X.; Fan, Y.; Qian, H.; Li, S.; Xiang, Y.; Ding, S. Surface plasmon resonance biosensor using hydrogel-AuNP supramolecular spheres for determination of prostate cancer-derived exosomes. *Mikrochim. Acta* **2020**, *187*, 590. [[CrossRef](#)] [[PubMed](#)]
43. Jin, D.; Yang, F.; Zhang, Y.; Liu, L.; Zhou, Y.; Wang, F.; Zhang, G.J. ExoAPP: Exosome-Oriented, Aptamer Nanoprobe-Enabled Surface Proteins Profiling and Detection. *Anal. Chem.* **2018**, *90*, 14402–14411. [[CrossRef](#)] [[PubMed](#)]

Disclaimer/Publisher’s Note: The statements, opinions and data contained in all publications are solely those of the individual author(s) and contributor(s) and not of MDPI and/or the editor(s). MDPI and/or the editor(s) disclaim responsibility for any injury to people or property resulting from any ideas, methods, instructions or products referred to in the content.